Supporting Information

Martínez et al. 10.1073/pnas.0911024106

SI Text

Thermofluor Measurements. TRα or TRβ (0.15 mg/mL) was added to TBS buffer [25 mM Tris (pH 7.5), 500 mM NaCl, and 1 mM DTT] containing a 1:2,000 dilution of Sypro orange (Invitrogen). Thirty microliters of buffer plus protein was added to each well of a 96-well MicroAmp plate (ABI). One microliter of either DMSO or a stock solution of 50 mM ligand in DMSO was added to each well. Using an ABI 7900 thermocycler, the temperature was raised from 25 °C to 80 °C at 4% of the maximum rate of the instrument. The resulting raw fluorescence traces were corrected for both the initial and final baselines. T_m's were determined by fitting the corrected melting curves to a 5-parameter sigmoidal dose–response curve using GraphPad Prism.

MD Simulations of Mutants. We conducted simulations with computational builds of TR LBC subtype specificity mutations (TRα-S277N and TRβ-N331S) to predict effects of Asn331Ser and Ser277Asn substitutions on pocket volume and water content. Arg-282β retracts to interact with the Ser backbone in the TRβ-N331S mutant, reducing LBC volume (Fig. S4*a*), and the Arg-320β side chain bends inward to adopt a position that resembles the A conformation of the TRβ x-ray structure (Fig. S4*b*). This event is accompanied by expulsion of a water molecule from the LBC (Fig. S4*c*). In the other simulation, the TRα-S277N substituent displaces Arg-228α so that it moves away from ligand and expands LBC volume. These data represent further evidence that Asn-331β and Ser-277α influence LBC volume and water content.

The computational builds of the mutants did not alter all TR subtype-specific aspects of the pocket. For complete binding mode reversal, the S277N mutation should alter Arg-320β side chain position to create a rigid bifurcated hydrogen bond with the Triac carboxylate, similar to that of Arg-266α and Triac. This was not observed. Likewise, strong hydrogen bond contacts between Arg-266α and Triac were preserved in the TRα-S277N mutant, precluding entrance of more water into the LBC. This may be a result of the computational limits of the present MD simulations.

Estimation of TRIAC Conformational Entropy Gain in TRβ Using Fluctuations in Ligand Position. The entropy of the system is a measure of the number of thermodynamically accessible microstates of a system (roughly, the number of energetically accessible conformations in the coordinate-velocity space, or phase-space). Given the number of accessible conformations, Ω, the entropy of the system can be computed by the classic Boltzmann formula:

$$S = R\, ln\, \Omega.$$

If 2 systems, A and B, have different numbers of accessible microstates, the variation in entropy associated with a transition from A to B can be computed by $S_B - S_A$, or

$$\Delta S = R\, ln\, (\Omega_B/\Omega_A).$$

Computing the relative number of accessible microstates yields the conformational entropy difference between the systems. This generally involves obtaining an ensemble of conformations for each system.

MD simulations can obtain such a conformational ensemble for a given molecular system. MD simulations providing an ensemble for which conformations are sampled according to the Boltzmann probability. The entropy, then, is related to the volume in phase-space occupied by the conformations obtained.

In practice, one extracts a finite sample of uncorrelated snapshots from the MD trajectory. The number of snapshots extracted is an arbitrary choice of the investigator and, therefore, is not related to the number of microstates of the system. A clustering algorithm capable of distinguishing and counting molecular conformations is used to estimate the conformational volume in phase space.

Here, we obtain an estimation of the conformational entropy difference of Triac in the binding pocket of TRα and TRβ from our MD trajectories. To cluster the conformations extracted from the MD simulations, we use a variation of the colony method described in ref. 1.

In ref. 1, one is interested in predicting likely loop conformations from an unknown protein structure. According to the method, one constructs a plot of some relevant energetic measure as a function of the rmsd relative to a reference structure for each system to provide a means for identifying (visualizing) the conformational colonies. Because the conformations in ref. 1 are generated from a loop-predicting algorithm, a probability function must be parameterized to weight each conformation according to its energy and the density of states in its vicinity (1). In our case, the MD simulations directly provide an ensemble of conformation with Boltzmann probabilities. The parameterized weighting procedure used in ref. 1 is, therefore, unnecessary here, but we can use a variation of their approach to count the number of ligand-conformational microstates in each subtype.

Fig. S6 displays the colony graph (1), in which the interaction energy between the ligand and the environment (protein + water + ions) is plotted as a function of the corresponding rmsd values relative to native structure.

As expected, Triac conformations in TRα are distributed around a single attractor (related to the snuggled attachment of the ligand's carboxylate group to Arg-266). In contrast, Triac presents 2 distinct conformational basins in TRβ owing to the different conformations it can assume in the TRβ binding pocket. As in ref. 1, we assume that the conformational ensemble is well represented by this 2D colony distribution and that the structural changes that are not distinguishable by the above representation do not differentiate microstates.

To estimate the conformational entropy in each case, one counts the number of different accessible microstates. A microstate is represented in Fig. S6 by an element of area. Each area element specifies a small range of energies and rmsds within which one considers conformations to be equivalent. The density of points within each element of area is representative of the *population* of the microstate. By measuring the area occupied by black dots in Fig. S6 (or, equivalently, the number of area elements occupied by at least a single conformation), we estimate the number of distinguishable accessible microstates obtained in the ensemble of our MD simulations.

To estimate the area occupied by the colony distributions depicted in Fig. 1, we use a box-counting algorithm. An equally spaced grid is drawn over the above 2D distributions, as illustrated in Fig. S7. A binary variable (1 or 0) is attributed to each bin: an occupied bin (i.e., bins with at least 1 black dot) takes on a value 1, whereas an empty bin is attributed a value 0. The total number of occupied bins provides an estimate for the number of relevant conformations in each colony.

Once the number of states occupied by the conformations of Triac in TRα (n_α) and TRβ (n_β) are computed, the difference in

conformational entropy of the ligand can be estimated from the Bolztmann entropy relation:

$$\Delta S = R\,ln\,(\Omega_\alpha/\Omega_\beta) \approx \mathrm{R\ ln}\,(n_\alpha/n_\beta) \quad [1]$$

and the free energy gain resulting from this entropic difference, ($\Delta G = -T\Delta S$) is, therefore, given by

$$\Delta G = -RT\,ln\,(n_\alpha/n_\beta). \quad [2]$$

It is important to note that grid size affects counting in this procedure. Let us assume that a very coarse grid is used, say, a grid that contains only 1 large bin. The state counting in both TRα and TRβ cases will equal 1, because all points fall within the single bin. In contrast, if an infinitely fine grid is used, each occupied bin will contain exactly 1 conformation, and the counting will yield the number of structures extracted from the MD simulations, which is the same for both subtypes (i.e., 3,000 in these calculations). Therefore, it is necessary to sample with varying grid sizes to access the range of grid size that best distinguishes conformations from colonies of both subtypes. Fig. S7 displays the box-counting results and the associated thermodynamic variables as functions of grid size. Fig. S8*a* shows that there are in general more populated states TRβ than in TRα. The ratio between these numbers (Fig. S8*b*) starts at 1 (for a grid composed of a single bin), reaches a maximum value at ≈250 bins, and decreases asymptotically toward 1 as the grid size increases to infinity, as expected (in this limit, both, n_α and n_β, approach 3,000). Grid sizes in the range of 200–300 bins distinguish best the conformational states from the 2 subtype colonies. The maximum value of n_β/n_α is ≈2 (Fig. S8*b*) and reflects the fact that the conformational dispersion of Triac in TRβ is roughly formed by 2 attractors with a dispersion similar to the single TRα attractor.

Fig. S8*c* shows that the resulting conformational entropy difference for the ligand between the 2 subtypes ranges from zero to a maximum of approximately 1.48 cal K^{-1} mol^{-1}. The corresponding free-energy difference at 298.15 K ranges from zero to 0.44 kcal mol^{-1}, as shown in Fig. S8*d*.

The experimental affinity measurements indicate that Triac is approximately 2- to 3-fold selective toward TRβ. Therefore,

$$K_{b,\beta}/K_{b,\alpha} \sim 2 \text{ to } 3,$$

and the corresponding range of free-energy difference, from $\Delta\Delta G = -RT \ln (K_{b,\beta}/K_{b,\alpha})$, is

$$\Delta\Delta G \sim -0.45 \text{ to } -0.65 \text{ kcal mol}^{-1}.$$

The estimated gain in free-energy provided by the increased conformational entropy of Triac in TRβ can account for a significant part of the observed β selectivity.

Most importantly, our analysis indicates that the ligand mobility differences observed in the simulations are associated with entropy gains that imply affinity enhancements of the order of the experimental value. The conformational flexibility of the protein and of water molecules, which are much more difficult to evaluate quantitatively, may have additional contributions.

1. Xiang Z, Soto CS, Honig B (2002) Evaluating conformational free energies: The colony energy and its application to the problem of loop prediction. *Proc Natl Acad Sci USA* 99:7432–7437.

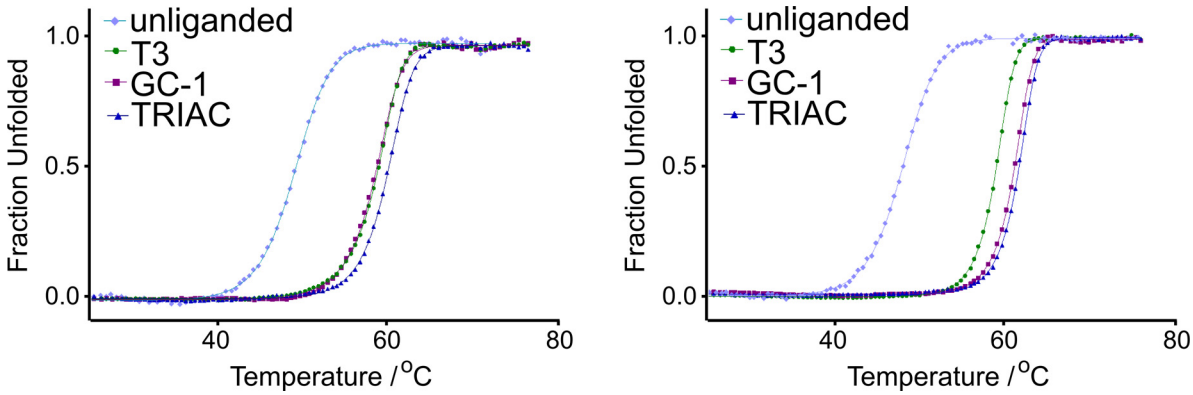

Fig. S1. Representative thermal denaturation curves for TRα (*Left*) and TRβ (*Right*) uncomplexed (light blue lines) and bound to T_3 (green), GC-1 (purple), and Triac (dark blue). The TRβ-Triac complex is stabler than the equivalent TRα-Triac complex or TRβ-GC-1 and TRβ-T_3 complexes.

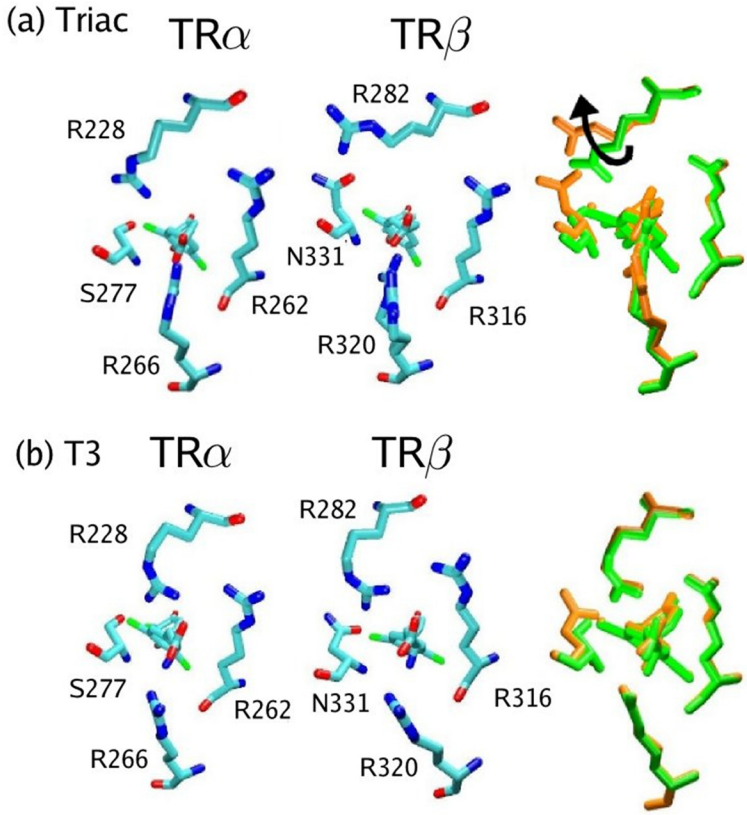

Fig. S2. Expansion of the TRβ pocket is specific to TRIAC. (*a*) With Triac, the conformations of the Arg-228/282 residue in each subtype are different, because it interacts with the side chain of the Ser-277/Asn-331 residue. This results in a larger binding cavity for TRβ, as described in the main text. (*b*) For T_3, the side chain conformations are similar between TR subtypes, because Arg-228/282 interacts directly with the ligand and not with the Ser-277/Asn-331 amino acid residue. These differences from the organization observed with Triac arise from the shorter carboxylate backbone of Triac relative to T_3 and mean that LBC volumes are similar for both TRs with T_3.

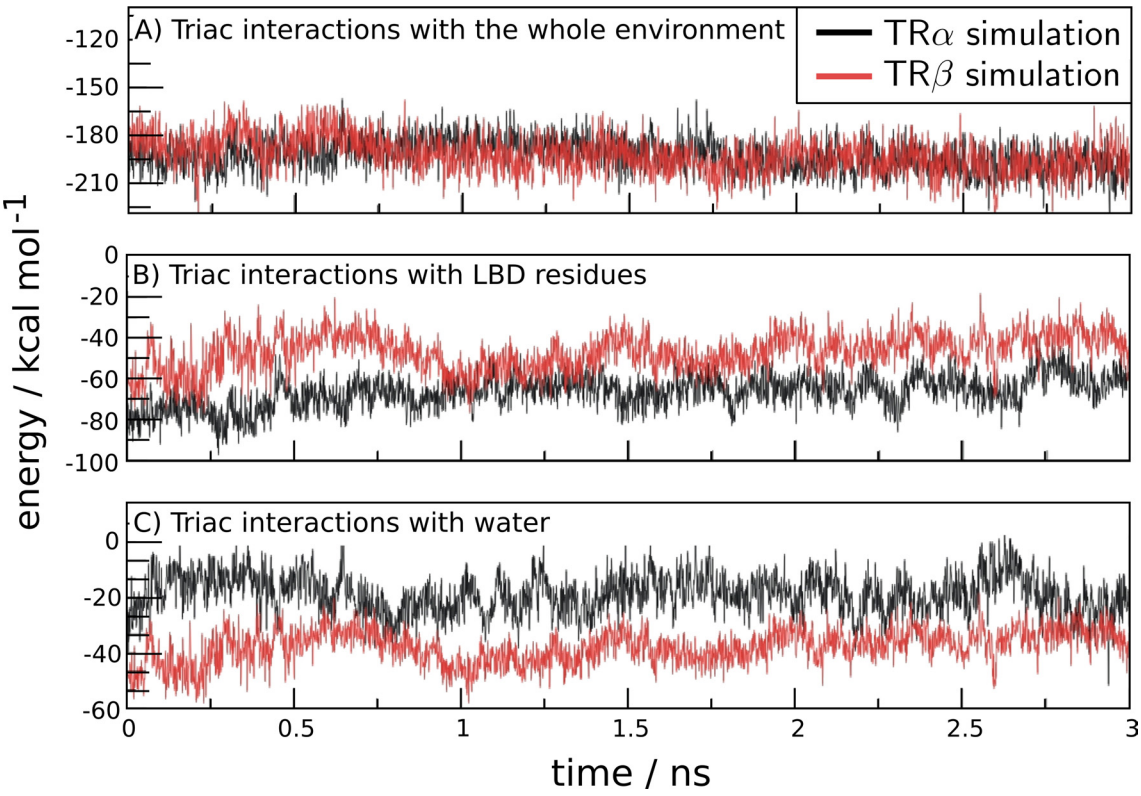

Fig. S3. Temporal evolution of the interaction energy of Triac with (*A*) the whole environment (protein + water + ions), (*B*) with LBD residues, and (*C*) with water molecules. Results for TRα and TRβ are shown in black and red, respectively. The energy values averaged over the entire simulations are summarized in Table 2 of the main text. There are no obvious differences in Triac interaction energies with both systems (*A*), but ligand interacts more tightly with TRα protein (*B*, black trace) vs. TRβ protein (*B*, red trace), whereas Triac interacts more tightly with water in the TRβ system (*C*, red trace) than in the TRα system (*C*, black trace).

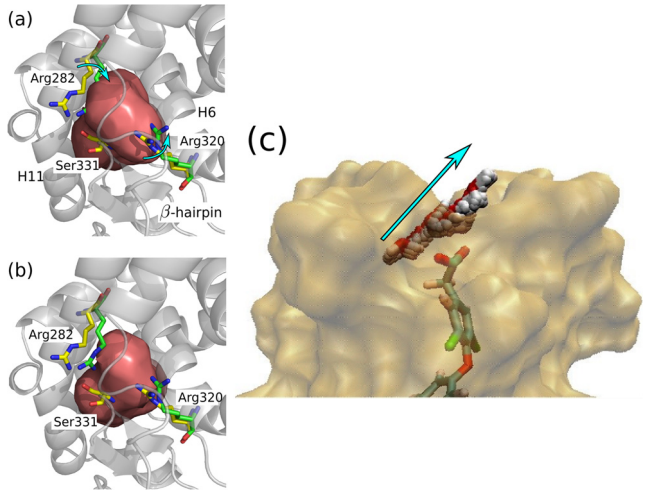

Fig. S4. Simulations with TR mutants to determine effect of the Asn331Ser mutation on TRβ LBC conformation. (*a*) Close-up view of the TRβ LBC (pink) in space-filling form, with key Arg side chains marked. Arg-282β and Arg-320β side chain conformations at the beginning of the simulation are equivalent to wild-type TRβ and are marked in yellow. New side chain positions that occur as a result of introducing a targeted mutation (Asn331Ser) are complete by 50 ps of the 3-ns simulation. New side chain positions are shown in green, with directions of movement highlighted with cyan arrows. Note that the new side chain position of Arg-282β is buried in the LBC. (*b*) Similar view of TRβ, with a space-filling model of the TRα LBC (pink) superimposed. Note that the TRα LBC fits well with the new side chain positions. (*c*) Reduction in LBC volume is accompanied by expulsion of a water molecule. The figure represents superimposed frames of a lateral view of the TRβ Asn331Ser mutant LBD throughout the simulation, with ligand position marked. Positions of a water molecule at various times are shown, with the direction of water movement marked with an arrow.

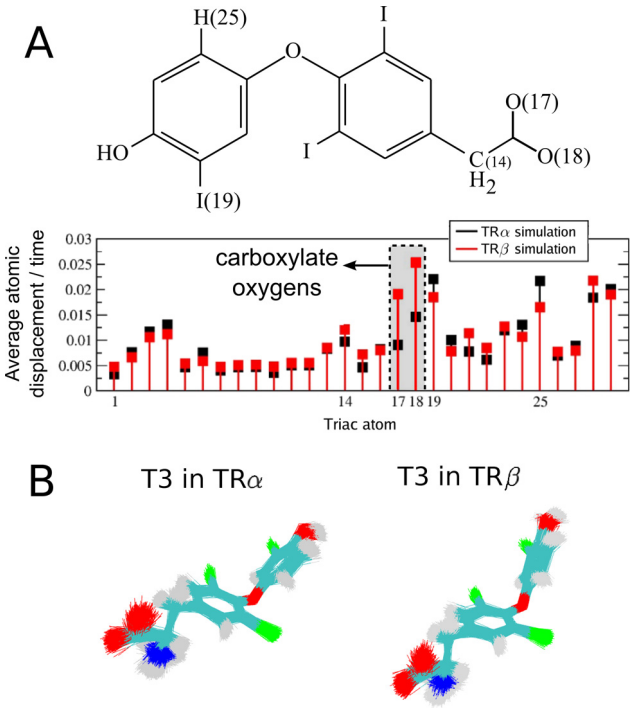

Fig. S5. (*A*) Average displacement of Triac atoms as a function of time. RMSD per time unit (ps) for each Triac atom (by number) in hTRα and hTRβ, showing greater mobility for Triac carboxylate (atoms 17 and 18) in TRβ. *Inset*: Triac with positions of atoms 17 and 18 labeled. (*B*) T3 exhibits similar mobility in TRα or TRβ.

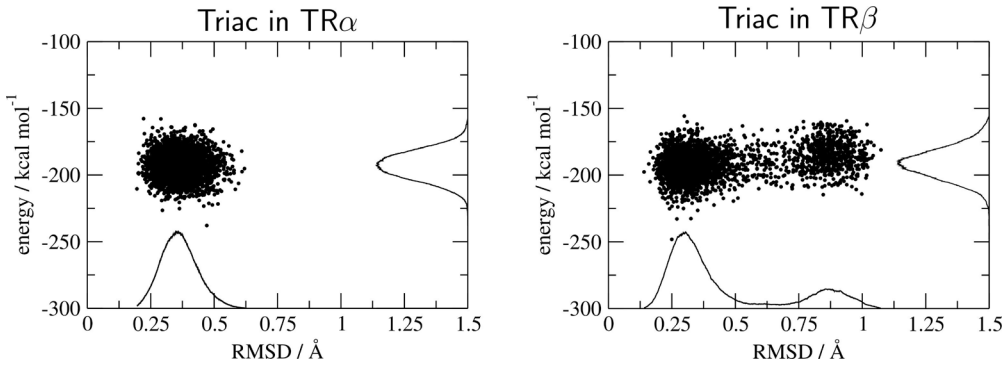

Fig. S6. Conformational ensembles of Triac in the binding pockets of TRα (*Left*) and TRβ (*Right*) as representations of conformational colonies (1). The curves in the *x*- and *y*-axes are rmsd and ligand-environment interaction energy distributions. A total of 3,000 MD snapshots were used for each system.

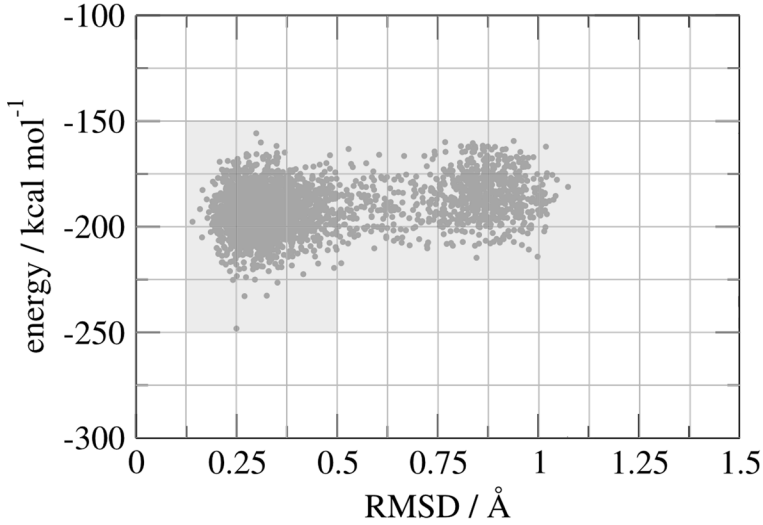

Fig. S7. Counting the number of occupied bins provides a means of estimating the number of thermodynamically relevant microscopic states in conformational colony space.

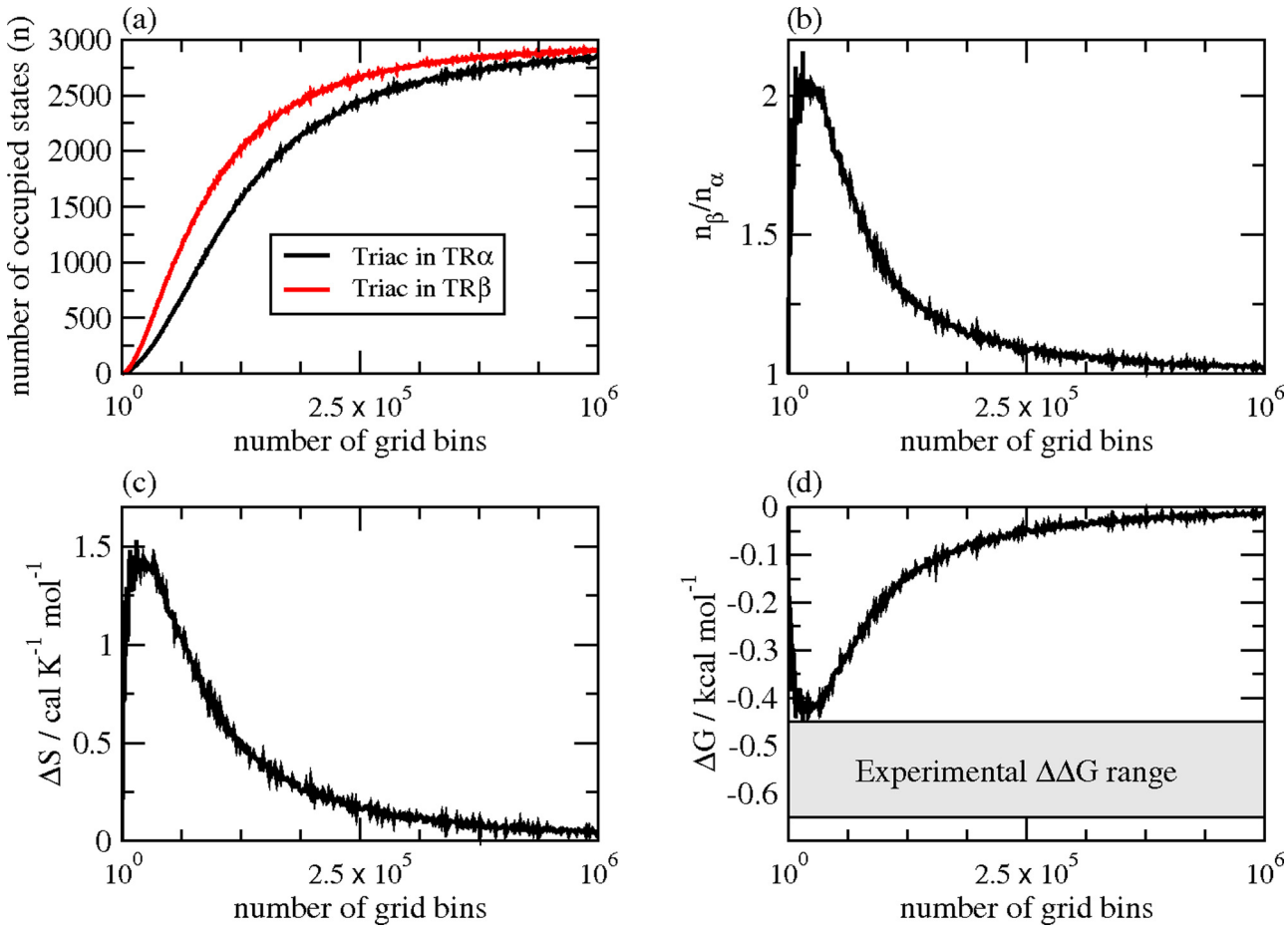

Fig. S8. Box-counting of states and associated thermodynamic values.

Table S1. Range of melting temperatures from multiple determinations

	Melting temperatures/°C (celsius degrees)			
TR	Unliganded	T3	GC-1	Triac
TRα	49.57–49.71	59.53–59.59	59.30–59.40	60.77–60.85
TRβ	48.90–49.09	60.38–60.42	62.58–62.65	63.14–63.20

Table S2. Data collection and refinement parameters

Parameter	hTRα	hTRβ
Wavelength (Å)	1.54 (rotating anode)	1.54 (rotating anode)
Space group	$P2_12_12_1$	$P3_121$
Resolution (Å)	38.95–2.0 (2.10–2.0)	29.79–2.50 (2.64–2.50)
Unit cell parameters (Å)	a = 60, b = 80, c = 102	a = b = 68, c = 131
Total no. of reflections	389,434 (45,846)	122,512 (17,858)
No. of unique reflections	33,965 (4,218)	12,993 (1,875)
Completeness (%)	97.8 (84.9)	100 (100)
Redundancy	11.5 (10.9)	9.4 (9.5)
Merged I/σ(I)	24.0 (2.9)	23.0 (2.9)
I/σ(I)	8.0 (0.9)	7.5 (1.0)
R_{merge}*	0.082 (0.817)	0.083 (0.763)
R_{pim}†	0.036 (0.374)	0.041 (0.379)
Total no. of atoms	2,011	2,401
R_{Factor}	0.196	0.174
R_{Free}	0.242	0.197
RMS bond lengths (Å)	0.008	0.015
RMS bond angles (°)	1.157	1.740

*$R_{merge} = \Sigma_{hkl} \Sigma_i |I_i(hkl) - <I(hkl)>| / \Sigma_{hkl} \Sigma_i I_i(hkl)$.

†R_{pim} (precision indicating R_{merge}) $= \Sigma_{hkl} [1/(N-1)]^{1/2} \Sigma_I |I_i(hkl) - <I(hkl)>| / \Sigma_{hkl} \Sigma_i I_i(hkl)$.